



## Study of Damaged Zone around Circular Opening Using Acoustic Emission Technique

A. Dadi Givshad, M. Ahmadi\* and H.R. Nejati

*Rock Mechanics Gr., Mining Dept., Eng. Faculty, Tarbiat Modares University, Tehran, Iran*

Received 18 December 2018; received in revised form 10 December 2019; accepted 1 February 2020

### Keywords

*Excavation damaged zone*

*Circular opening*

*Acoustic emission technique*

*FLAC3D software*

### Abstract

One of the methods used to investigate the damaged zone in rock structure is the acoustic emission method. This method is based on receiving the elastic waves that are produced by deformation and cracking of the rock mass around the underground excavation. In this research, a study is conducted on the rock samples by a numerical method to investigate the damaged zone caused by the excavation of circular space on it. For this purpose, 33 cube samples of three different material types including sandstone, concrete, and cement-plaster mortar are prepared. A circular hole is drilled in the center of each sample. The hole diameter is 20 or 25 mm. The samples are loaded uniaxially or biaxially with different stress rates. It is tried to study the acoustic events occurring in the samples during the test, and their locations are investigated. Then the experiments are evaluated by a numerical method using the FLAC3D software and some developed codes. The relation between the sample damaged zone where the acoustic events have occurred during the loading period and the numerical elements that reach a degree of tensile and shear yield is studied. The results obtained show that the amount of cumulative acoustic parameters in cement-plaster mortar specimens is more than the others. In fact, the finer grains, the more amounts of energy and counts will be produced. Also, the results show that with increase in the lateral pressure and loading rate, the amount of cumulative energy and counts decreases.

### 1. Introduction

The propagation of damage around underground excavations could lead to fractures. This changes hydraulic and mechanical properties of the rock mass surrounding the underground excavations. Thus, it is important to study the damaged zone in the underground excavations, particularly for waste disposal. The damaged zone in an underground excavation in the civil and dam construction projects could result in irreversible outcomes. It is impossible to excavate an underground space near the foundation without identifying the damaged zone, because the excavation changes stress on the rock mass around excavation [1-3].

From a theoretical view, the excavation damaged zone, starts at the excavation surface and develops to an extent where the physical, mechanical, and

hydro-mechanical characteristics of rock mass change. Formation of a damaged zone is very sensitive to the development and propagation of micro-cracks [1, 4].

Several physical and numerical methods have been presented to identify EDZ, each of which has an especial complication and require more research works. Nowadays, acoustic emission (AE) is used as a non-destructive method for determination and evaluation of the damaged zone [1, 5]. Acoustic events are created in propagation of the elastic waves caused by deformation and crack initiation. This method can be used for evaluation of damage in the rock around the excavation [5]. In this research, the hollow cube samples are built, and by laboratory and numerical methods, excavation damage zone is investigated.

Corresponding author: [moahmadi@modares.ac.ir](mailto:moahmadi@modares.ac.ir) (M. Ahmadi).

## 2. Literature review

As it is shown in Figure 1, excavation damage zone is divided into 3 separate zones as HDZ, EDZ, and EdZ. HDZ consists of large-scaled fractures and crushed rocks. The greatest amount of damage occurs in underground excavation in

this area. Induced stresses are responsible for damage in EDZ. In this zone, changes such as deformation, permeability, and initial stresses happen to rock mass. In the case of EdZ, the induced stresses are not enough for micro-crack initiation, so the damage is reversible [1].

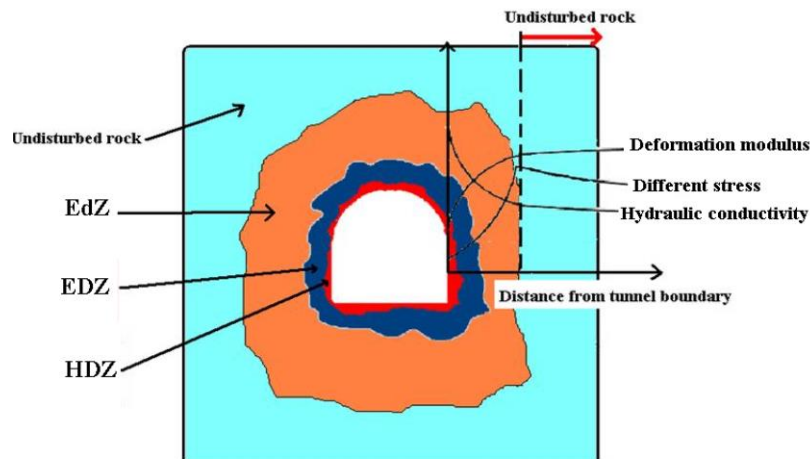


Figure 1. Various zones around an underground excavation [1].

Since the initiation and propagation of cracks are always accompanied by acoustic emission waves, Zhang *et al.* (2006) have proposed equation 1 to define the relation between the acoustic parameter and the damage variable (D) [6]:

$$D = \frac{\Omega}{\Omega_m} \quad (1)$$

Where  $\Omega_m$  is a cumulative number of an acoustic emission parameter such as hits, counts, amplitudes or energies determined when the sample is destroyed, and  $\Omega$  is the cumulative number of the same acoustic emission parameter

during a damage process and  $0 \leq \Omega \leq \Omega_m$  or  $0 \leq D \leq 1$  [6].

A biaxial compression test has been performed by Fakhimi (2002) on a sandstone specimen with a circular opening to simulate a loading-type failure around an underground excavation in a brittle rock, and a failure process has been detected by the AE technique. He showed that the micro-crack pattern in the numerical model (PFC<sup>2D</sup>) was compatible with the locations of AE determined in a laboratory test (Figure 2) [7].

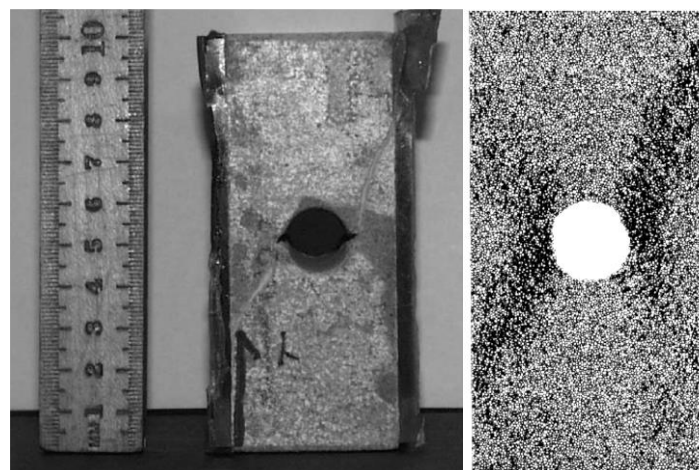


Figure 2. Damaged pattern in laboratory sample and numerical model [7].

Zhu (2005) has shown that for a circular opening under uniaxial compression or a low lateral pressure coefficient, a primary tensile crack, a

remote tensile crack, and a shear crack develop. For a lateral pressure, the coefficients are less than 0.25, the applied stresses are required to form the

primary tensile crack, and for excavation, collapse increases with increasing lateral pressure. When the lateral pressure coefficient is 0.75 or 1.0, no primary tensile crack develops, and the state of stress at the initiation of shear damage increases with the lateral pressure [8, 9].

In order to simulate the failure process around the underground excavations in brittle rocks, Wang (2012) has used a perforated sample, and utilized the finite element code RFPA<sup>2D</sup> to model the failure process. He recognized that the results of numerical modeling and AE events were in good matchings [10]. He applied different values of confining pressures ranging from 3 to 11 MPa to

study the effect of variation in confining pressure on the circular hole. The results obtained indicated that the tensile cracks were the main reason of failure when the value of confining pressure was low (3 MPa), while for higher confining pressures (5 and 7 MPa), the quantity of tensile cracks decreased and the shear cracks caused failure. This behavior can be explained by the high values of confining pressures, which prevent the initiation and propagation of the tensile cracks. He showed that the cumulative number of AE events decreased with a higher confining pressure (Figure 3) [10].

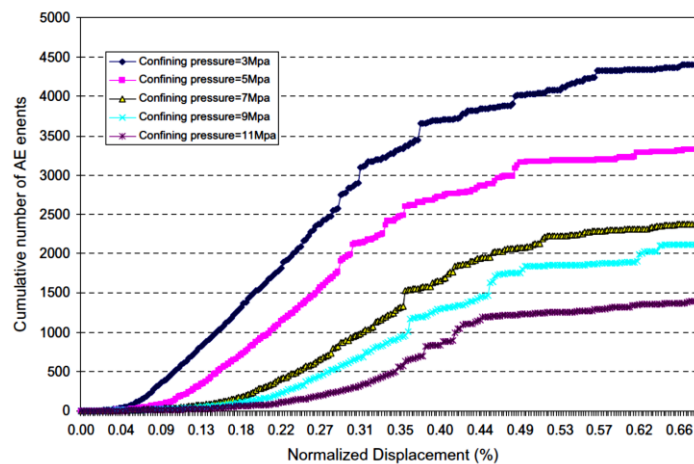


**Figure 3. Numerically simulated results of the cumulative number of AE events versus normalized displacement (displacement/height) of specimens with confining pressures [10].**

Zhao (2014) have shown that when granite blocks containing one pre-existing cylindrical cavity are loaded in an uniaxial compression condition, the profiles of cracks around the cavity can be characterized by tensile cracking (splitting parallel to the axial compression direction) at the roof-floor, compressive crack at two side walls, and remote or secondary cracks at the perimeter of the cavity. Moreover, the fracture around cavity is size-dependent. In granite blocks containing multiple parallel cylindrical cavities, the adjacent cylindrical cavities can influence each other, and the eventual failure mode is determined by the interaction of tensile, compressive, and shear stresses [11].

Liu (2015) created D-shape holes in granite samples and conducted AE experiments on them. He used the moment tensor for locating the AE events. He noticed that during the loading process, the initiated micro-cracks were divided into the three categories of shear mode, tensile mode, and mix mode. About 60% of the cracks are of shear mode, while less than 30% are of tensile mode.

The shear mode cracks occur on the walls but tensile cracks initiate on the crown [12].

Xu (2017) have studied the process of damage and crack initiation in granite samples using the moment tensor, showing that crack initiation and failure happen in the zone where there is a stress concentration. He showed in his experiments that for circular cavities, shear cracks were dominant with a percentage more than 45%, and tension cracks were fewer, accounting for less than 40% of the total events. He showed that the tensile failure occurred on the crown and bottom, while shear failure appended on the walls [13].

### 3. Sample preparation and testing

In this research, the cube shape samples with dimensions of  $150 \times 150 \times 150$  mm were built to study the damaged zone due to an underground excavation. As presented in table 1, the selected materials for the samples were sandstone, concrete, and cement-plaster mortar. As the next step, a circular hole with different diameters of 20

and 25 mm were drilled in the center of each sample.

A Santam loading machine with capacity of 100 tons and precision of 0.04 micrometer deformation was used for applying uniaxial stress on the samples. It is a self-controlled device, and is able to apply load on the samples with a constant rate. The displacement rate in the

uniaxial tests was 0.2 to 0.8 (mm/min). It also can automatically record the stress and strain magnitude during the loading and unloading time (Figure 4). The AE device was Vallen system GmbH Co., which had 4 sensors for data acquisition and planar analyzing, and produced some acoustic parameters, e.g. cumulative counts and energy.

**Table 1. Material type and loading type**

No.	Material type	Loading type	Number of test
1	Sandstone	uniaxial	10
2		biaxial	5
3	Cement-plaster mortar	uniaxial	10
4	Concrete	uniaxial	8

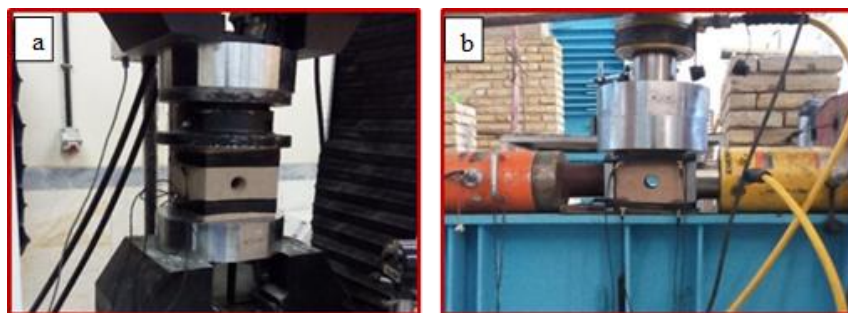


**Figure 4. Uniaxial (a) and biaxial (b) loading on cube sample with hole.**

Three patterns of acoustic sensor location in the samples were proposed for data acquisition. It should be mentioned that pattern A was chosen as the ideal pattern, and was used for uniaxial loadings. Pattern B was also used for biaxial loadings because placing a sensor in the center of

samples was not possible. Pattern C was not utilized in the study because of the existence of a continuous void in the center of samples, and recording acoustic data was not correct. The patterns are shown in Figure 5.

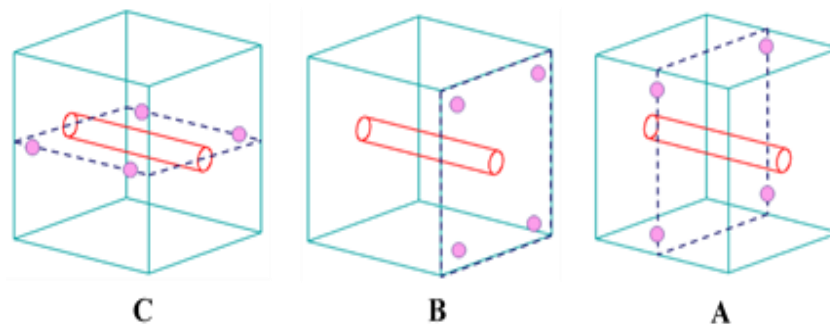


**Figure 5. Different patterns for locating acoustic sensors on the samples.**

In this study, 33 tests were conducted on the samples with different hole diameters under uniaxial and biaxial loading conditions with distinctive displacement rates.

**4. Analysis of experiments**

**4.1. Analysis of AE parameters**

The process of uniaxial and biaxial loading on perforated cube samples and cumulative curves of

energy and counts for acoustic events during loading is indicated in Figures 6 to 8. The primary results of the experiments on the samples are presented in Table 2. It should be noted that the porosity of the concrete specimens is much more than the porosity of the sandstone and plaster specimens, which significantly influence the failure mechanism of the specimens.

In the next step, in order to analyze the experimental results, it was tried to draw cumulative counts and cumulative energy vs. different loading rates in two different hole diameters. Also variations in different material

sample strength, cumulative energy, and cumulative counts vs. increasing the lateral pressure in different hole diameters were drawn. These curves are presented in Figures 9 to 11.

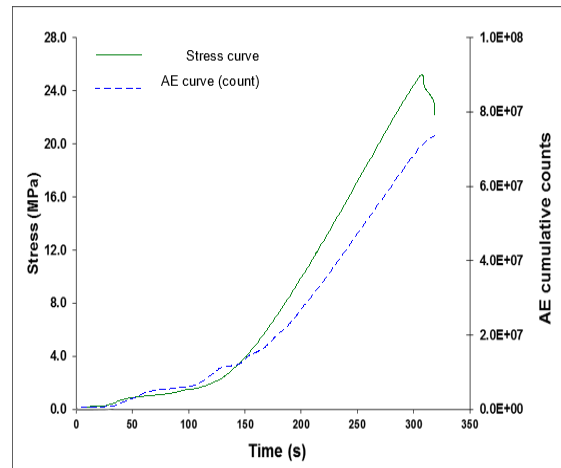
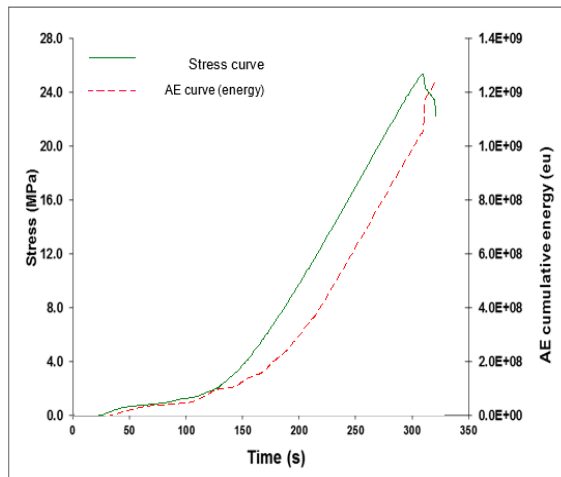


Figure 6. Cumulative energy and counts vs. time and stress vs. time for sandstone sample.

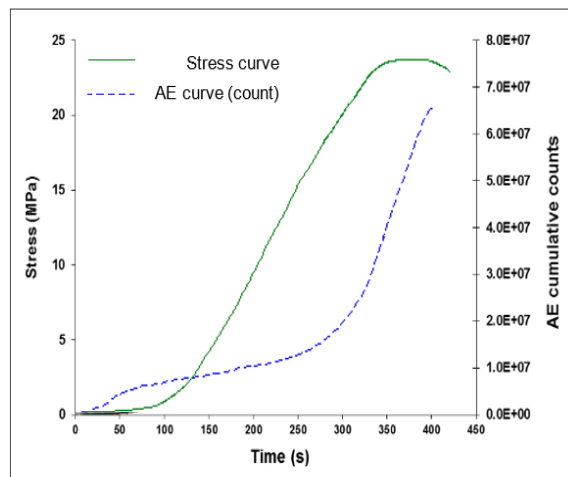
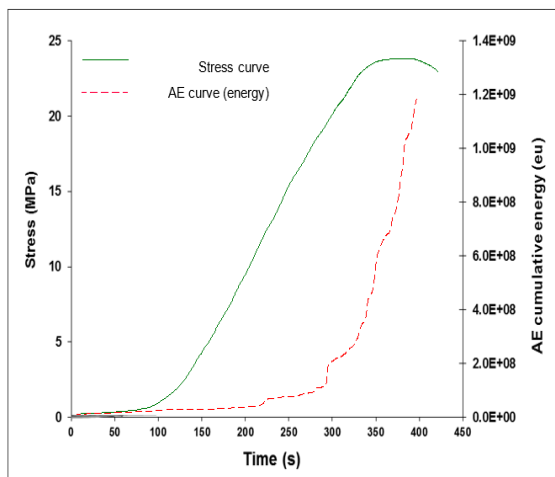


Figure 7. Cumulative energy and counts vs. time and stress vs. time for concrete sample.

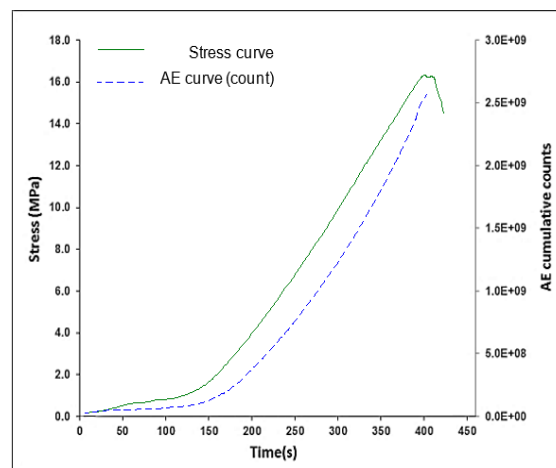
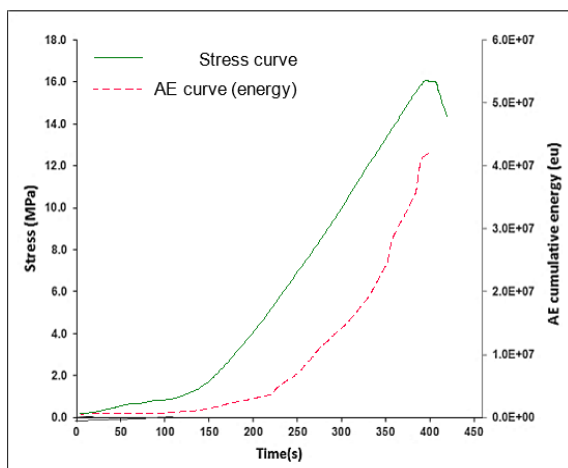
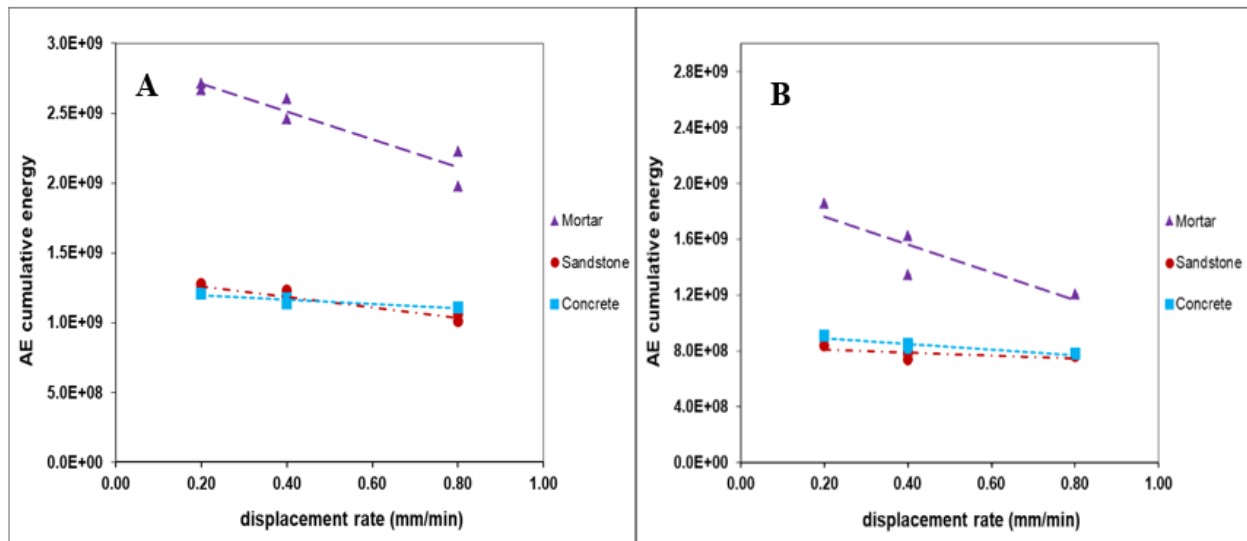


Figure 8. Cumulative energy and counts vs. time and stress vs. time for cement-plaster mortar sample.

**Table 2. Primary results of tests and AE data.**

Test No.	Material type	Loading type	Diameter hole (mm)	Displacement (mm/min) rate	lateral pressure (MPa)	Strength (MPa)	Acoustic parameters			
							Cumulative count	Cumulative hit	Cumulative energy	
1	Sandstone	uniaxial	25	0.2	0	21.9	$8.8 \times 10^7$	$5.1 \times 10^5$	$12.8 \times 10^8$	
2						22.4	$8.2 \times 10^7$	$4.7 \times 10^5$	$12.4 \times 10^8$	
3						23.5	$7.4 \times 10^7$	$3.5 \times 10^5$	$12.3 \times 10^8$	
4				0.4	0	22.8	$7.8 \times 10^7$	$3.9 \times 10^5$	$11.5 \times 10^8$	
5						23.5	$6.1 \times 10^7$	$2.8 \times 10^5$	$10.1 \times 10^8$	
6						24.2	$6.5 \times 10^7$	$3.0 \times 10^5$	$10.6 \times 10^8$	
7				0.8	0	23.8	$6.2 \times 10^7$	$3.1 \times 10^5$	$8.4 \times 10^8$	
8						24.3	$5.8 \times 10^7$	$2.9 \times 10^5$	$7.8 \times 10^8$	
9						25.1	$5.9 \times 10^7$	$2.7 \times 10^5$	$7.4 \times 10^8$	
10		biaxial	20	0.8	0	25.8	$5.7 \times 10^7$	$2.9 \times 10^5$	$7.6 \times 10^8$	
11						1.0	24.7	$3.2 \times 10^7$	$2.1 \times 10^5$	$2.3 \times 10^8$
12						3.0	27.5	$1.7 \times 10^7$	$8.1 \times 10^4$	$1.5 \times 10^8$
13						5.0	31.5	$1.1 \times 10^7$	$5.9 \times 10^4$	$7.0 \times 10^7$
14						1.0	25.6	$1.7 \times 10^7$	$8.5 \times 10^4$	$2.6 \times 10^8$
15						5.0	32.8	$9.6 \times 10^6$	$5.2 \times 10^4$	$1.1 \times 10^8$
16	Cement-plaster mortar	uniaxial	25	0.2	0	14.7	$9.5 \times 10^7$	$5.4 \times 10^5$	$27.2 \times 10^8$	
17						14.9	$8.7 \times 10^7$	$5.1 \times 10^5$	$26.7 \times 10^8$	
18						15.6	$9.0 \times 10^7$	$5.3 \times 10^5$	$26.1 \times 10^8$	
19				0.4	0	15.4	$8.1 \times 10^7$	$4.5 \times 10^5$	$24.6 \times 10^8$	
20						15.7	$7.4 \times 10^7$	$4.0 \times 10^5$	$22.3 \times 10^8$	
21						16.1	$7.7 \times 10^7$	$4.5 \times 10^5$	$19.8 \times 10^8$	
22				0.8	0	15.2	$7.7 \times 10^7$	$4.3 \times 10^5$	$18.6 \times 10^8$	
23						15.9	$8.5 \times 10^7$	$5.0 \times 10^5$	$16.3 \times 10^8$	
24						16.3	$7.1 \times 10^7$	$4.0 \times 10^5$	$13.5 \times 10^8$	
25				16.9	$6.9 \times 10^7$	$3.8 \times 10^5$	$12.1 \times 10^8$			
26	concrete	uniaxial	20	0.2	0	22.5	$7.1 \times 10^7$	$3.6 \times 10^5$	$12.1 \times 10^8$	
27						23.9	$6.7 \times 10^7$	$3.2 \times 10^5$	$11.7 \times 10^8$	
28						23.2	$6.5 \times 10^7$	$3.3 \times 10^5$	$11.4 \times 10^8$	
29				0.4	0	25.1	$6.6 \times 10^7$	$3.1 \times 10^5$	$11.1 \times 10^8$	
30						23.4	$5.4 \times 10^7$	$2.5 \times 10^5$	$9.1 \times 10^8$	
31						24.1	$5.1 \times 10^7$	$2.7 \times 10^5$	$8.2 \times 10^8$	
32				0.8	0	25.1	$4.6 \times 10^7$	$1.9 \times 10^5$	$8.5 \times 10^8$	
33						26.6	$4.1 \times 10^7$	$2.8 \times 10^5$	$7.8 \times 10^8$	



**Figure 9. Cumulative energy vs. displacement rate for different sample type (hole diameter; A: 25 mm, B: 20 mm).**

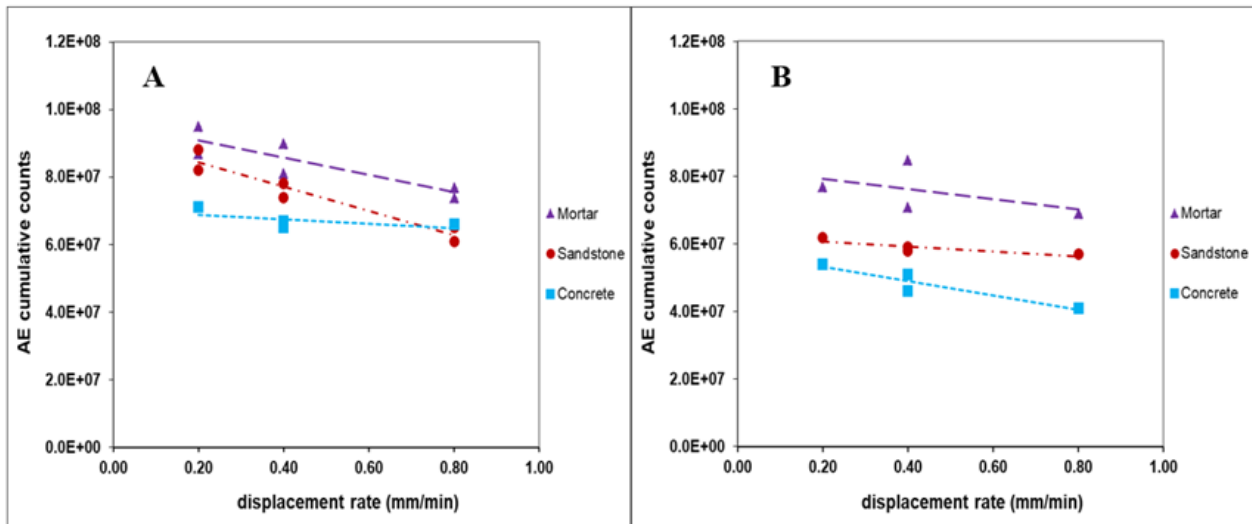


Figure 10. Cumulative count vs. displacement rate for different sample type (hole diameter; A:25 mm, B:20 mm).

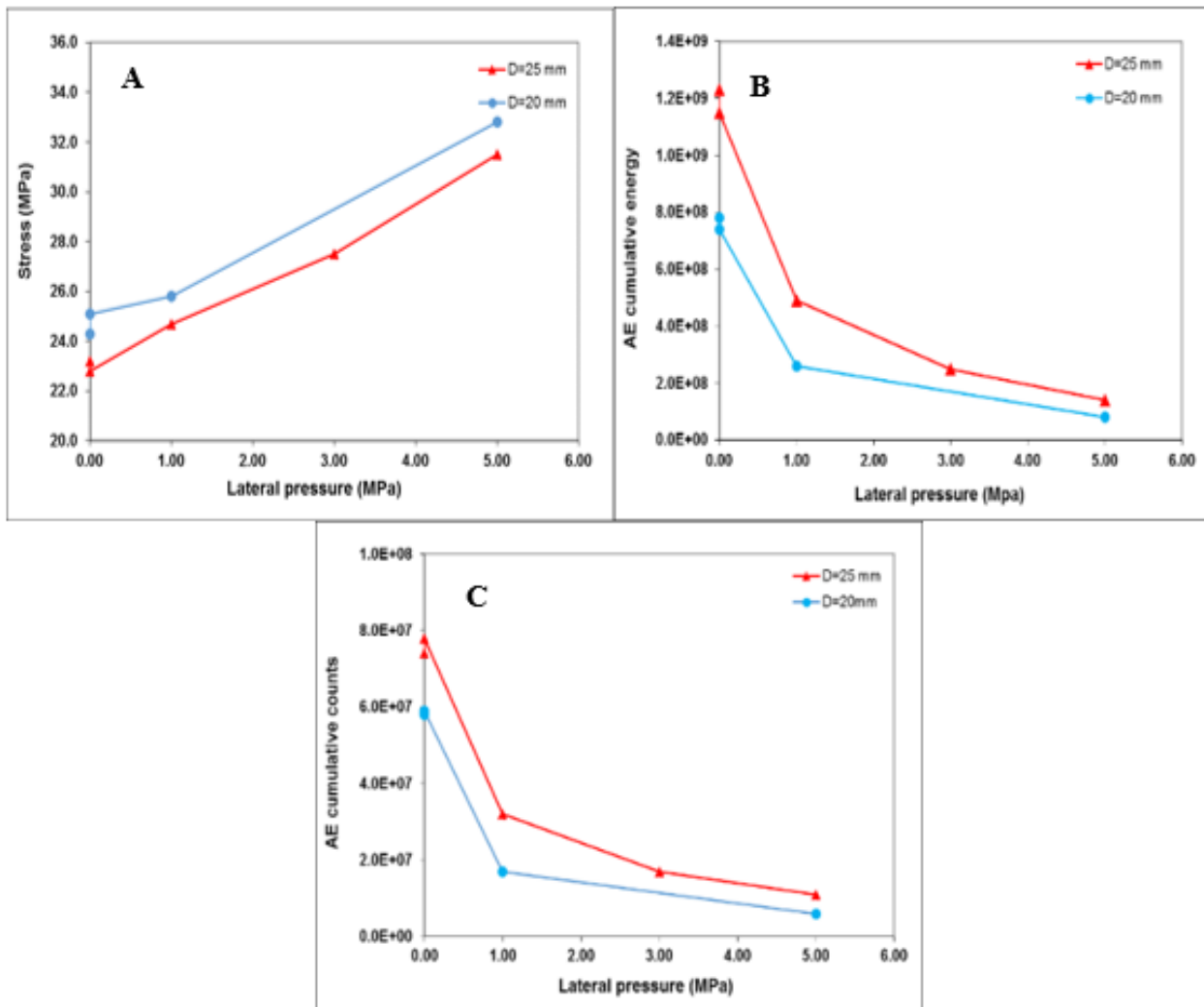


Figure 11. Variations in (a) sample strength, (b) cumulative energy, and (c) cumulative count with increasing lateral pressure in sandstone in different diameter holes.

It should be mentioned that the values of cumulative energy and count parameters in the cement-plaster mortar samples are generally greater than the other samples. The reason for this

behavior is that the cement-plaster mortar grain is finer than the other specimens. In fact, the aggregate levels of the seeds that are in contact with one another are greater related to the others

samples. Therefore, they have a higher ability to produce acoustic waves.

The results obtained showed that with increase in the loading rate, the amount of cumulative energy and counts decreased. Reduction in the values is greater for the cement-plaster mortar samples than the others sample. In fact, with increase in the loading rate, duration of stress in samples and cumulative acoustic parameter reduces. Therefore, small loading rate of 0.2 mm/min was chosen for the studied location.

In the following, by increasing the lateral pressure that increases the samples strength, cumulative values of energy and counts decrease due to the reduction in the total displacement of the samples and decrease in the movement of energy-producing grains. As noted, Wang also observed in his experiments that the cumulative number of AE events decreased with a higher confining pressure.

#### 4.2. Location analysis

The study of acoustic events location around the hole in the sample was one of the main objectives of this research. Different techniques are used to explain the process and location of the acoustic events, which describe how and where damage occurs in the rock media. The determination of events location is carried out by minimizing the interval between the received times of different waves of an event.

The basis for location calculation is the time-distance relationship implied by velocity of sound wave, which is called point location. The absolute arrival time ( $t$ ) of a hit in an event can be combined with the velocity of the sound wave ( $v$ ) to yield the distance ( $d$ ) from the sensor to the source [14]. Therefore:

$$d = vt \tag{2}$$

In this formula, the velocity is constant, and the distance between the source of unknown coordinates ( $x_0, y_0, z_0$ ) and sensor  $i$  with known coordinates ( $x_i, y_i, z_i$ ) can be found as [15]:

$$d_i = \sqrt{(x_i - x_0)^2 + (y_i - y_0)^2 + (z_i - z_0)^2} \tag{3}$$

The distance of the source to the sensor “ $i$ ” can also be given by [14]:

$$d_i = v(t_i - t_0) \tag{4}$$

Where  $t_i$  is the arrival time to sensor  $i$  and  $t_0$  is the time of event occurrence.

These calculations are complicated due to the lack of accurate knowledge of the occurrence time. To get around this problem, all the times are considered relative to the first hit of the event. Each arrival time difference implies a difference in distance to the sensor relative to the distance to the first hit [16, 17]. For the second sensor,  $i = 2$ , relative to the first sensor,  $i = 1$ , a difference equation can be written as [14]:

$$t_2 - t_1 = \frac{(d_2 - d_1)}{v} \tag{5}$$

Considering a 2D geometry (plane), where  $x_0$  and  $y_0$  are unknown coordinates of the source, Eq. 3 can be combined with Eq. 5 to yield:

$$t_2 - t_1 = [\sqrt{(x_2 - x_0)^2 - (y_2 - y_0)^2} - \sqrt{(x_1 - x_0)^2 - (y_1 - y_0)^2}]/v \tag{6}$$

This equation contains two unknowns ( $x_0$  and  $y_0$ ) and cannot be solved by itself. To get a second equation with the same two unknowns, a third sensor should be added to the produced equation:

$$t_3 - t_1 = [\sqrt{(x_3 - x_0)^2 - (y_3 - y_0)^2} - \sqrt{(x_1 - x_0)^2 - (y_1 - y_0)^2}]/v \tag{7}$$

These simultaneous equations can then be solved for  $x_0$  and  $y_0$ . The math becomes more complicated when extended to three dimensions (volumetric) but the approach remains the same [14].

Estimation of the hit location obtained from the data could contain errors due to different reasons. These errors can be investigated using the AE software by the “LUCY” graph. In fact, “LUCY” is named as the location uncertainty. It is possible to determine the uncertainty for every located acoustic event using the software. Since the accuracy of the acoustic event location is very important, estimation of the hit location that has an error value more than +/- 1 mm is not accounted for the following analysis [18].

A typical drawing of the acoustic event location during the loading period with a rate of 0.4 mm/min on the sandstone specimen is shown in Figure 12. The value of the maximum stress in each level was a percentage of the failure stress, meaning: level one; 10%, level two; 25%, level three; 50%, level four; 70%, level five; 80%, and level six; 100%.

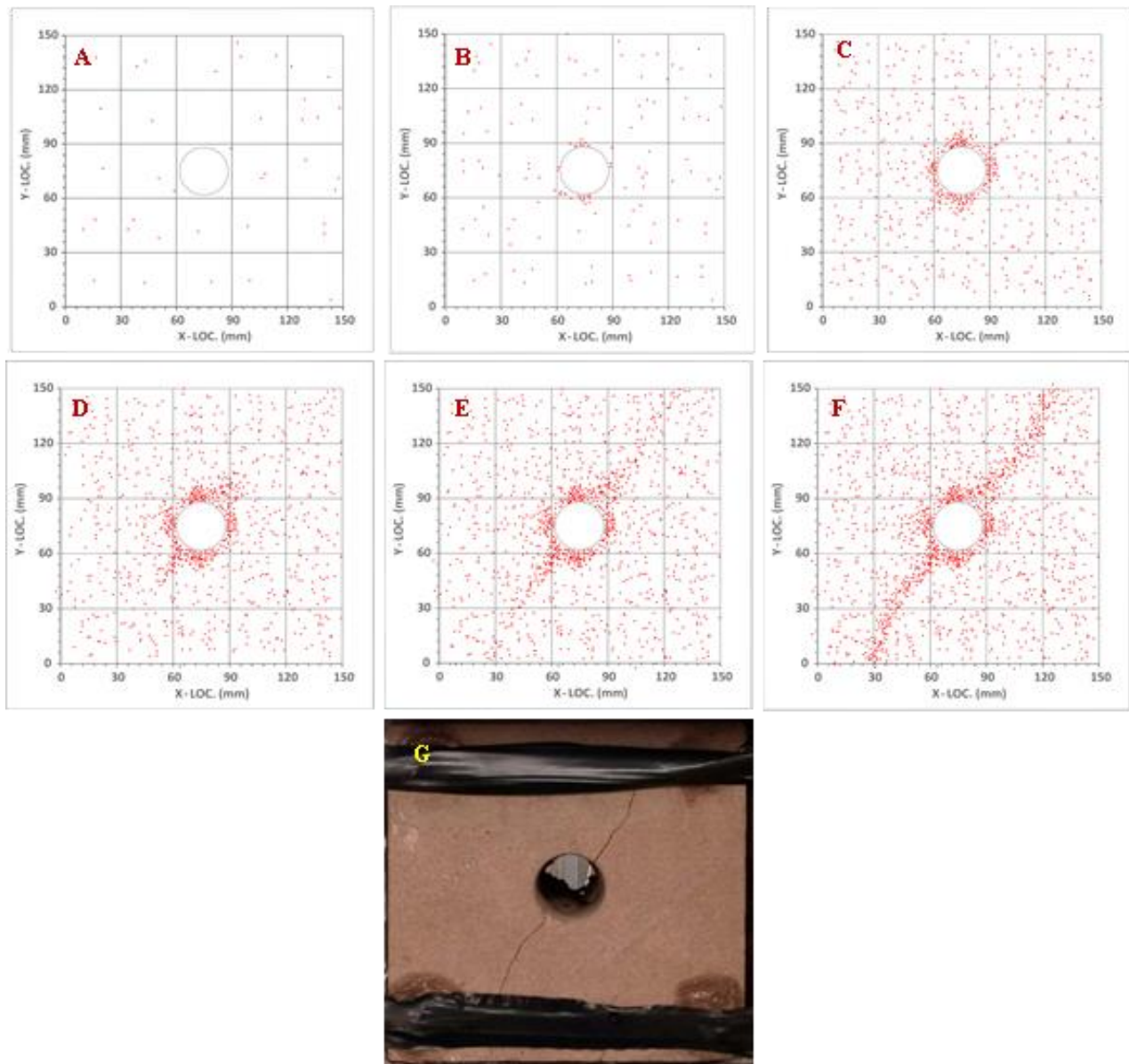


**Figure 12.** Acoustic event location in different loading steps (A:  $0.1\sigma_{cri}$ , B:  $0.25\sigma_{cri}$ , C:  $0.5\sigma_{cri}$ , D:  $0.7\sigma_{cri}$ , E:  $0.8\sigma_{cri}$ , and H:  $\sigma_{cri}$ ), and G: test No. 3.

As it is indicated in Figure 12, for level one, almost all the recorded acoustic events are stochastic and do not have a specific distribution pattern. In level two, the acoustic events are observed in the top and bottom of the hole. According to the rock mechanics analysis, these events are of tensile mode. For the stress value equal to half the failure stress meaning level three, the acoustic events increase in the top and bottom of the specimen, and in addition, the scattered acoustic events occur throughout the sample. Also a limited number of events are observed in the walls of the sample. The expansion of the acoustic events in the top and bottom of the specimen almost stops in level four. The acoustic events happen in a direction parallel to the diameter of

the specimen. In Figures 13 to 15, the examples of failures in the samples and the acoustic event location are observed. In this study, the damage observed in the laboratory samples was similar to the damage observed in the Fakhimi's experiments (Figures 2 and 12). More explanation regarding this subject will be presented after the numerical analysis.

### 5. Numerical analysis

In this research, a numerical method was used to better understand and complete the experimental works. The FLAC<sup>3D</sup> software was used for the numerical method. The experimental sample was simulated with the numerical model and the geomechanical properties of the samples were applied to the model. In order to verify the

numerical model, a comparison was made between the results of the numerical model and the experimental results. The relations between the zone where the acoustic events occurred

during the loading period in the sample and the zone (elements) in the numerical model that yielded shear or tensile were studied.

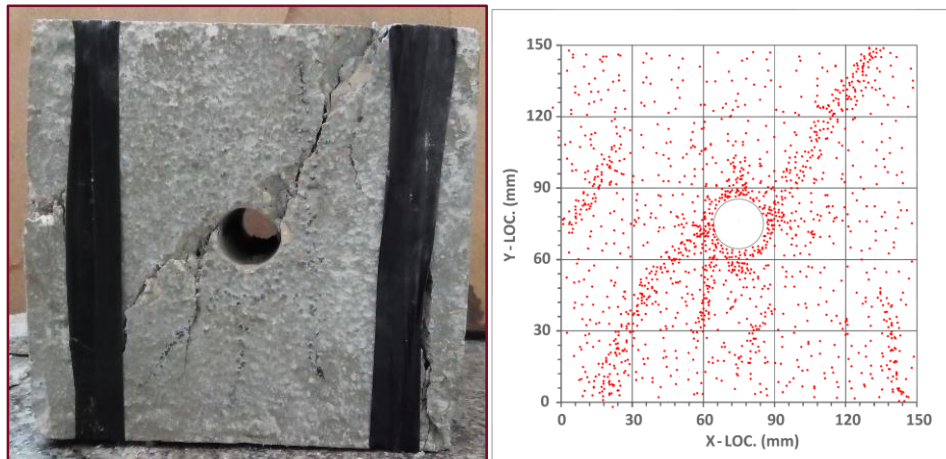


Figure 13. Acoustic event location in a concrete sample.

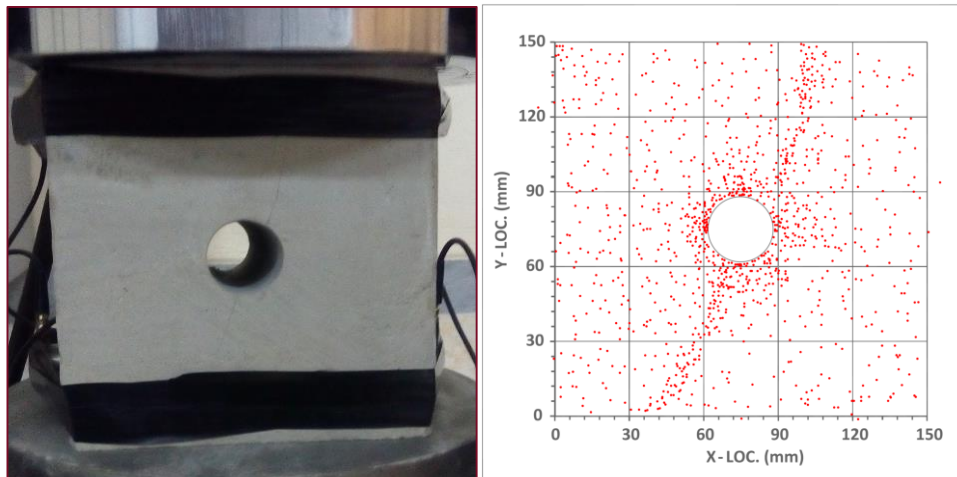


Figure 14. Acoustic event location in a cement-plaster mortar sample.

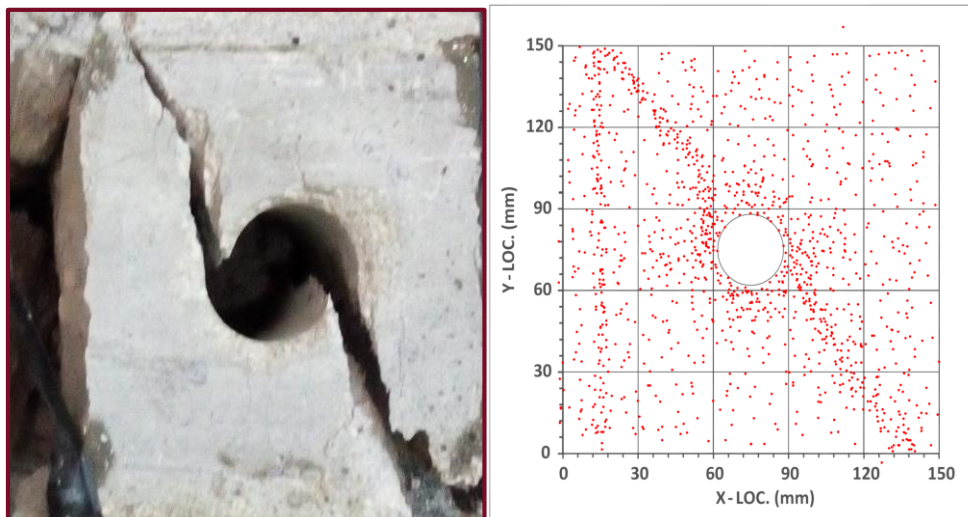


Figure 15. Acoustic event location in a concrete sample.

### 5.1. Heterogeneity in sample

Rock materials consist of different types of minerals (cement materials, voids, and micro-joints) that cause the rock to become heterogeneous. Some of the mentioned components have different physical and mechanical properties, which means that their reaction to loading will be different. Thus, it is necessary that this heterogeneity is considered in the numerical model; otherwise, a simplification in the numerical model will not provide a full

description of the damage process. Therefore, according to what was said, the spatial distribution of heterogeneity in rock samples could play a decisive role in the strain caused by loading period and controlling the failure stages [19, 20].

Liu (2004) has introduced the Weibull distribution function to describe heterogeneity in a rock. As shown in Figure 16, the Weibull distribution is a continuous probability distribution [19, 20].

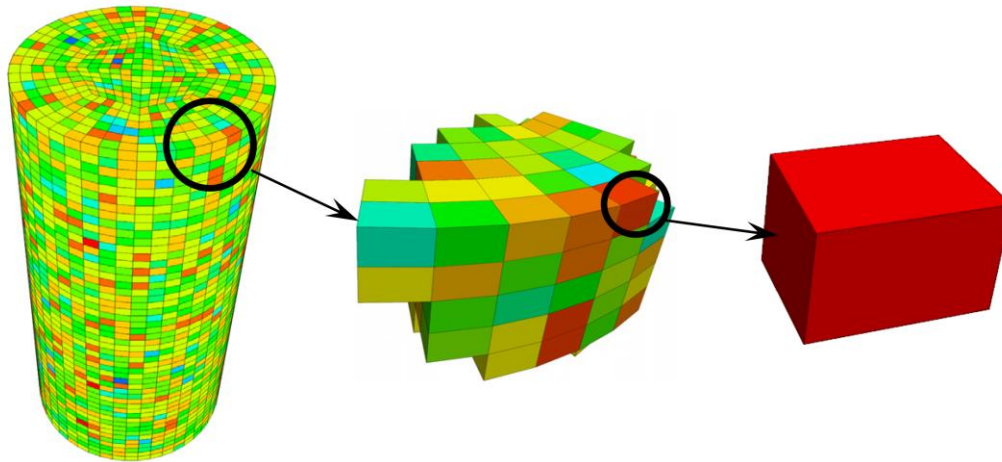


Figure 16. Heterogeneous spatial distribution in a numerical model in FLAC<sup>3D</sup> [19].

In this function, parameters of a numerical model could be defined randomly in the interval [0, 1]:

$$u = F(x) = 1 - \exp\left[-\left(\frac{x}{\beta}\right)^m\right] \quad (8)$$

The inverse form is:

$$x = F^{-1}(u) = \beta[-\ln(1 - u)]^{\frac{1}{m}} \quad (9)$$

Where  $u$  is the distribution function defined in FLAC<sup>3D</sup> using URAND,  $m$  is the heterogeneity index, and  $\beta$  is the model scale parameter [19].

In the numerical modeling, in order to achieve more realistic results comparable to those obtained from the laboratory tests, the heterogeneous distribution for the geomechanical parameters such as cohesive, internal friction angle, and tensile strength was used. To apply the inherent heterogeneity of the samples in order to obtain perfect results, a code based on the above equations was developed, and was performed using the FLAC<sup>3D</sup> software. Therefore, each element in the numerical model was randomly assigned geomechanical parameters with a scattering value. In fact, with the code, heterogeneity in the geomechanical parameters of samples could be defined in the numerical model.

### 5.2. Study of damaged zone

In order to investigate the damaged zone in FLAC<sup>3D</sup>, it is necessary to choose the yield or failure criterion. The Mohr-Columbian criterion was selected because it had a good conformity with the rock behavior. This criterion is presented in Equation 10. In the software, to show the area of yield or failure, in other words, damaged zone, it uses the strength to stress ratio. In the software, this ratio is calculated instantaneously, and its previous value is not considered in the loading period. Therefore, a special code was developed and was performed in the software, which could calculate the ratio at each stage of loading for the shear or tensile failure mode separately. It should be noted that another application of this code is the safety factor calculation at each loading step. In the software, the compressive stress is assumed with a negative sign and the tensile stress with a positive sign. Therefore, according to the criterion, the ratio of strength to stress can be determined by Equation 11.

The Mohr-Coulomb criterion is provided in Equation 10. In FLAC<sup>3D</sup>, the compressive stress is assumed as a negative value, while the tensile stress is considered as a positive value. The ratio

of strength to stress could be defined by means of Equation 11 based on this criterion [21].

$$\sigma_{1f} = \left( \frac{1 + \sin(\varphi)}{1 - \sin(\varphi)} \right) \sigma_3 - 2C \sqrt{\frac{1 + \sin(\varphi)}{1 - \sin(\varphi)}} \quad (10)$$

In the above equation, f is safety factor in shear failure. According to equation 11, this ratio could be calculated for shear failure in each element of the numerical model in each loading step and the elements that achieved the specified coefficient [21]. According to equation 11, this ratio could be calculated for shear failure in each element of the numerical model in each loading step and the elements that achieved the specified coefficient [21].

In order to calculate the safety factor in the zone affected by tensile stress, elements with a positive value of minor stress ( $\sigma_3$ ) are identified, and the safety factor is calculated according to Equation (12).

$$F = \frac{\sigma_t}{\sigma_3} \quad (12)$$

In order to compare the results obtained from the numerical model and the laboratory sample, it is required to develop a specific code and performed in the software according to Equation 12. The code can independently calculate and plot the ratio of strength to shear or tensile stress at each loading step for each element cumulatively.

The strength to the stress ratios of 1, 1.3, 1.6, and 2 were chosen, and the zones with this ratio were displayed separately. The relation between these zones and the sample zones where acoustic events occurred during the loading period were

evaluated. In fact, the acoustic events occur due to (1) sliding of grains, and (2) crack initiation or propagation in the rock specimens.

### 5.3. Numerical modeling

In this part of the study, the results of the laboratory tests were reviewed by constructing the numerical models. To achieve this, the mechanical parameters of the laboratory sample (e.g. strength, elasticity modulus) were applied to the numerical models, and then these models were adapted according to the laboratory results. For example; in Figure 17, stress vs. displacement curve in the experimental and the numerical model is shown. In total, for all experiments, there was a maximum of 10% difference between the parameters of the numerical and laboratory models ( $\sigma_c$  and displacement).

Following adaptation of the numerical models, the relation between the elements of a numerical model that reached a degree of shear or tensile yielding was investigated with zone of laboratory samples that acoustic events occurred during loading.

The numerical models were executed by considering the heterogeneity coefficients of 2, 10, 20, and 100, and the loading steps in which the stress was 10, 25, 50, 70, 80, and 100 percent of failure stress and the strength-stress ratios of 1, 1.3, 1.6 and 2 and stress-strain curve of each case was plotted. The tensile and shear failure zones with the above assumptions for a sandstone sample (test No. 4) as a representative of results are presented in Figures 18 to 21.

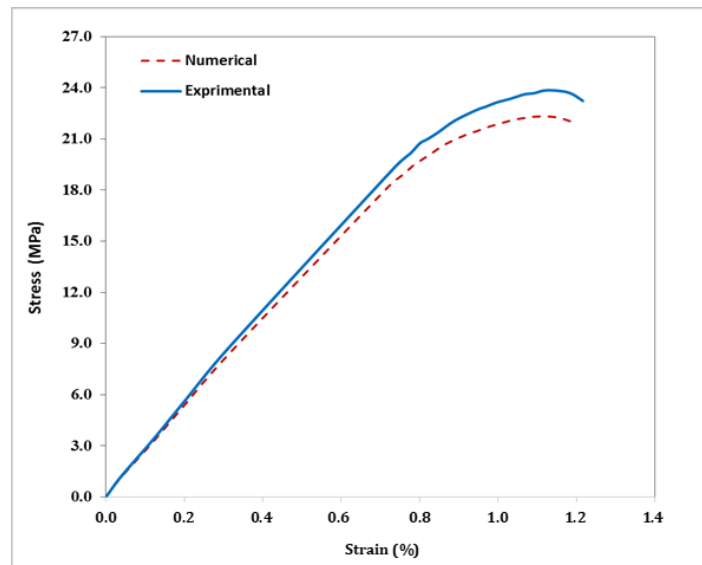
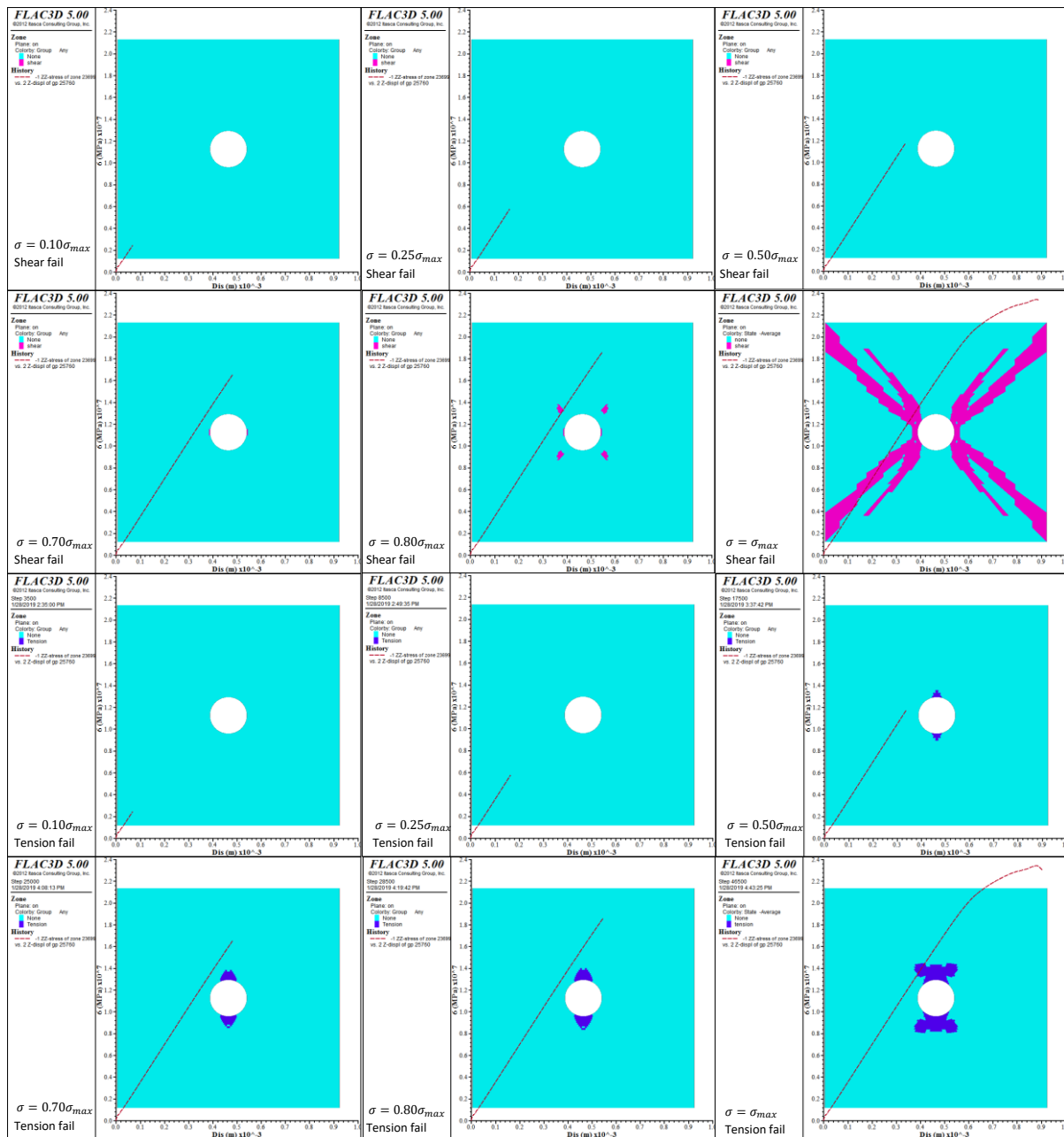


Figure 17. Stress vs. strain curve in the experimental and numerical model.



**Figure 18. Tensile and shear yield zone of heterogeneous numerical model with applying coefficient of strength to stress ratio equal to 1.**

As indicated in Figure 18, zones of tensile failure were observed in the top and bottom of the specimen along direction of loading when the model was assumed homogenous under a stress equal to half the specimen strength. In this step, no shear failure zone was observed in the sample. It should be noted that although the tensile failure zone at the specimen's top continued to expand during the next loading steps, they did not affect the model's final failure process.

When the applied load to model was increased to 70% of the specimen's strength, shear failure zones were observed in the walls of the specimen hole. In the final steps of loading, the failure zone was observed along the specimen's diameter. As noted, Zhao (2014) and Xu (2017) in their experiments showed that tensile cracking at the roof-floor and shear crack took place at two side-walls.

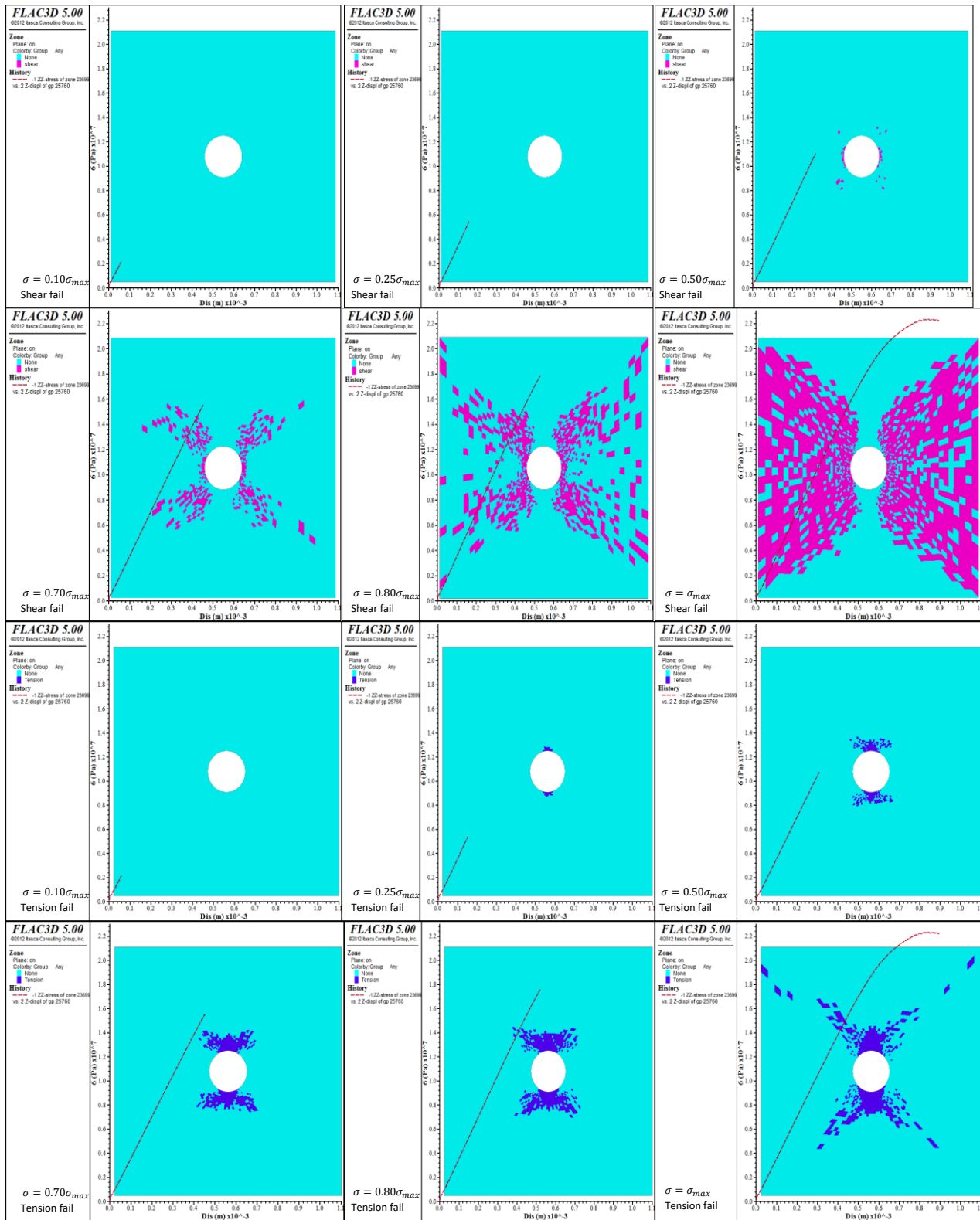


Figure 19. Tensile and shear yield zones of non-homogeneous numerical model ( $m = 20$ ) by applying coefficient of strength to stress ratio equal to 1.3.

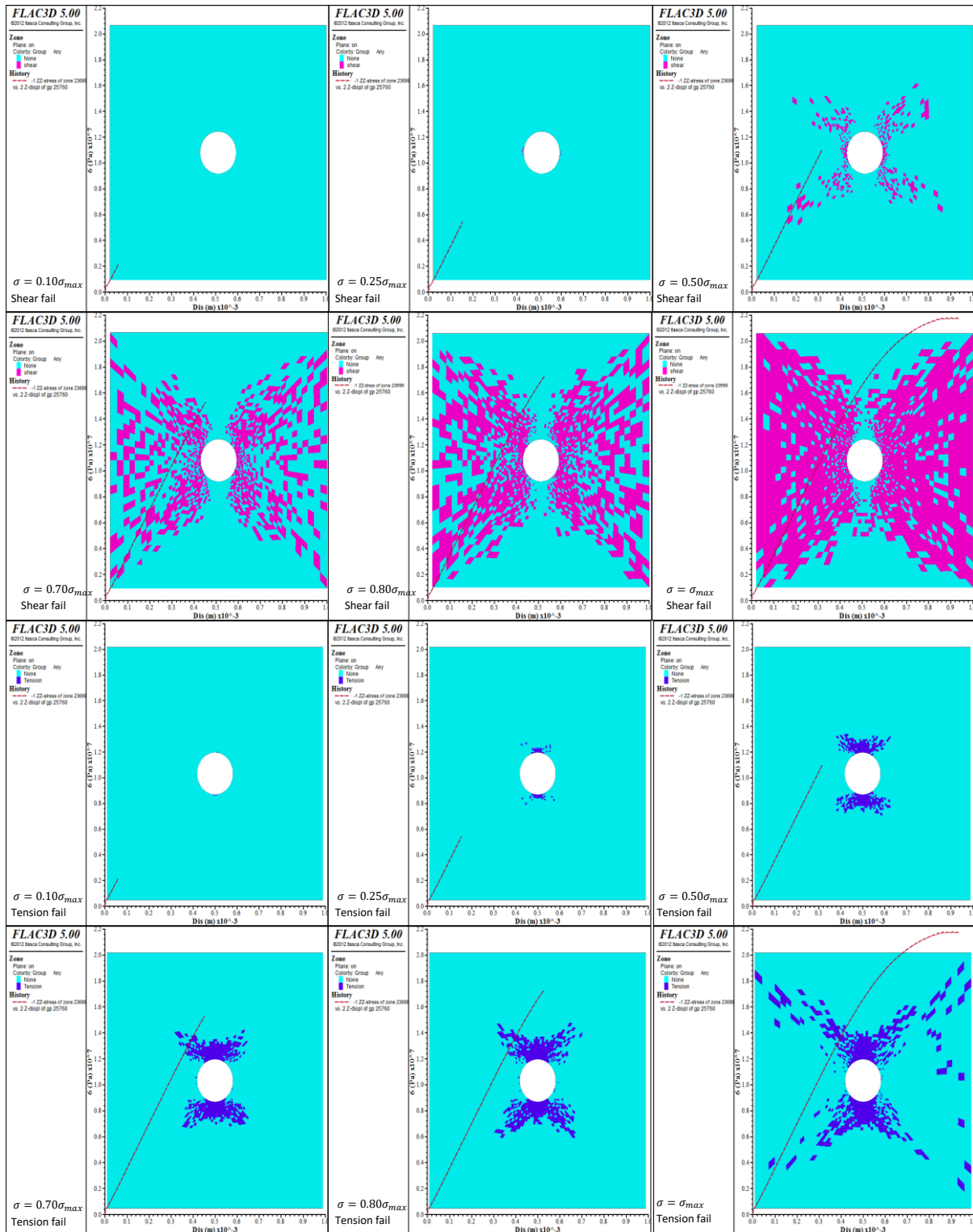


Figure 20. Tensile and shear yield zones of non-homogeneous numerical model ( $m = 10$ ) by applying coefficient of strength to stress ratio equal to 1.6.

As it can be seen in Figures 18 to 21, when the specimen is more heterogeneous and the ratio of strength to stress is higher, the initiation of tensile and shear failure zones occurs in a smaller stress. The correlation coefficient between the results of acoustic events in laboratory specimens and

tensile and shear zone in numerical model is presented in table 3.

As shown in the 3, up to 10% of the failure stress, the events are random and there is no clear relationship between the observed acoustic events in laboratory specimens and yield zone in the numerical model.

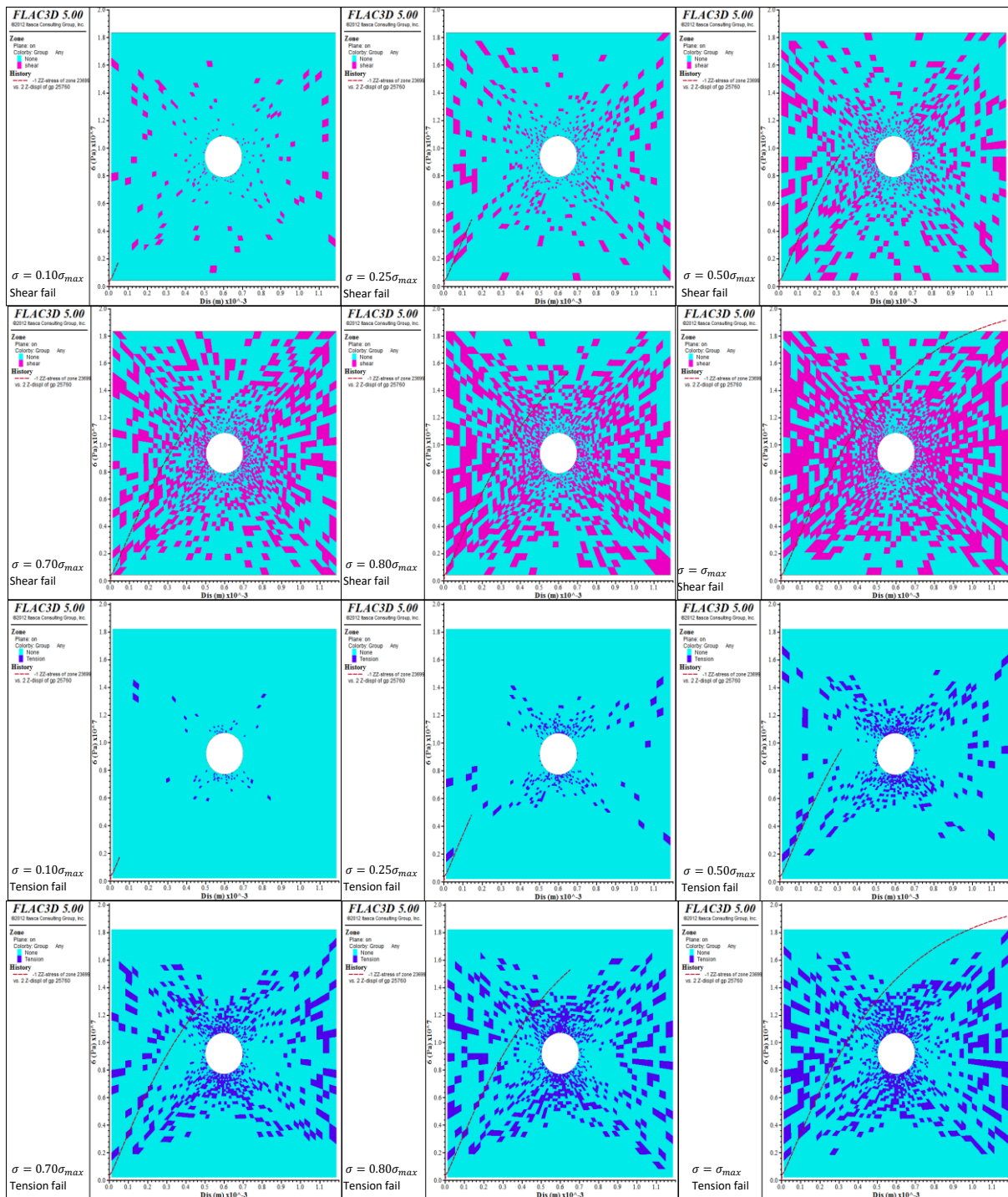


Figure 21. Tensile and shear yield zones of non-homogeneous numerical model ( $m = 2$ ) by applying coefficient of strength to stress ratio equal to 1.6.

The results obtained also showed that the correlation coefficient increased when applying the heterogeneity coefficient and the strength to stress ratio in the numerical model. It should be noted that in the cement-plaster mortar samples, there is a better correlation between the acoustic events in laboratory samples and the yield zone in numerical model than in the sandstone samples and concrete samples.

Based on the results obtained from this study, for the sandstone and cement-plaster mortar model, it is recommended that the strength to stress ratio and the heterogeneity coefficient are defined as 1.3 and 20, respectively, and for the concrete model, the strength to stress ratio and the heterogeneity coefficient are 1.3 and 10, respectively.

**Table 3. Correlation coefficient between results of the acoustic events in laboratory specimens and tensile and shear yield zone in numerical model.**

Material type	Strength to stress ratio (tensile and shear)	Correlation coefficient						
		Stress to failure stress percentage						weighted average
		10%	25%	50%	70%	80%	100%	
Sandstone	1.0 (homogeneous)	0.00	0.00	0.25	0.32	0.41	0.48	0.34
	1.3 (heterogeneity coefficient =20)	0.00	0.65	0.72	0.84	0.86	0.72	<b>0.75</b>
	1.3 (heterogeneity coefficient =10)	0.00	0.62	0.69	0.76	0.77	0.71	0.70
	1.6 (heterogeneity coefficient =10)	0.00	0.69	0.61	0.65	0.67	0.65	0.63
	1.6 (heterogeneity coefficient =2)	0.82	0.77	0.52	0.53	0.56	0.49	0.55
Cement-plaster mortar	1.0 (homogeneous)	0.00	0.00	0.29	0.35	0.42	0.55	0.38
	1.3 (heterogeneity coefficient =20)	0.00	0.71	0.79	0.88	0.87	0.75	<b>0.79</b>
	1.3 (heterogeneity coefficient =10)	0.00	0.67	0.74	0.77	0.80	0.75	0.73
	1.6 (heterogeneity coefficient =10)	0.00	0.75	0.62	0.69	0.70	0.66	0.66
	1.6 (heterogeneity coefficient =2)	0.85	0.78	0.59	0.58	0.62	0.53	0.60
Concrete	1.0 (homogeneous)	0.00	0.00	0.22	0.28	0.40	0.45	0.32
	1.3 (heterogeneity coefficient =20)	0.00	0.59	0.66	0.81	0.79	0.67	0.70
	1.3 (heterogeneity coefficient =10)	0.00	0.66	0.72	0.78	0.84	0.72	<b>0.74</b>
	1.6 (heterogeneity coefficient =10)	0.00	0.65	0.58	0.62	0.65	0.60	0.60
	1.6 (heterogeneity coefficient =2)	0.72	0.70	0.45	0.52	0.50	0.45	0.50

**6. Conclusions**

In this study, the acoustic emission (AE) technique was used for evaluation of the damaged zone around underground opening. To achieve this purpose, 33 cube samples were prepared from 3 different materials and a circular hole with different diameters was drilled in the center of each sample, and then the uniaxial and biaxial tests were conducted in the laboratory.

The AE parameters during the loading of samples were studied, and the locations of acoustic events were detected. In the next step, FLAC3D software was used for more investigation of the damaged zone around the openings. A numerical modeling was developed using the fish function and the locations of AE events in experimental models were compared with the yielded zone of the numerical simulation. The conclusions of this study can be summarized as follow:

1. With increase in the loading rate, the recorded AE events decreased in different specimens. Then when a small loading rate (0.2 mm/min) was chosen for testing, the location of the events was

predicted with more accuracy than the other loading rates.

2. The default yielding criterion in FLAC produced a small plastic zone around the openings, which did not have a good correlation with the AE locations detected in the experimental specimens. However, on the basis of the heterogeneity coefficient and strength to stress ratio, a new numerical model was developed using the FLAC fish functions. The results of the numerical modeling revealed that there was a good correlation between the AE locations detected in the experimental specimens and yielded zones in the developed numerical model.

3. The appropriate value for strength to stress ratio in the developed models was 1.3 for all the three different types of specimens (concrete, cement-plaster mortar and sandstone).

4. The heterogeneity coefficient is an influencing parameter for evaluation of the damaged zone around the opening, and the specimens with more heterogeneity possessed a larger damage zone around the openings.

5. An appropriate value for the heterogeneity coefficient of sandstone and cement-plaster mortar was 20, while the concrete specimens had more heterogeneity and the relevant heterogeneity coefficient was 10 for the understudied concrete specimens.

## 7. References

- [1]. Fattahi, H., Shojaee, S. and Farsangi, E. (2013). Application of adaptive neuro-fuzzy inference system for the assessment of damaged zone around underground spaces. *International journal of optimization in civil engineering*, 3 (4): 673-693.
- [2]. Tsang, C.F., Bernier, F. and Davies, C. (2005). Geohydraulic processes in the excavation damaged zone in crystalline rock, rock salt, and indurated and plastic clays—in the context of radioactive waste disposal. *International Journal of Rock Mechanics and Mining Sciences*, 42 (1): 109-125.
- [3]. Sato, T., Kikuchi, T. and Sugihara, K. (2000). In-situ experiments on an excavation disturbed zone induced by mechanical excavation in Neogene sedimentary rock at tono mine, central Japan. *Engineering Geological*. 56 (2): 97-108.
- [4]. Shen, B. and Barton, N. (1997). The disturbed zone around tunnels in jointed rock masses. *International Journal of Rock Mechanics and Mining Sciences*, 34 (1): 117-125.
- [5]. Suzuki, K., Nakata, E., Minami, M., Hibino, E., Tani, T., Sakakibara, J. and Yamada, N. (2004). Estimation of the zone of excavation disturbance around tunnels, using resistivity and acoustic tomography. *Exploration Geophysics*, 35 (1): 62-69.
- [6]. Ji, M., Zhang, Y.D., Liu, W.P. and Cheng, L. (2014). Damage evolution law based on acoustic emission and Weibull distribution of granite under uniaxial stress. *Acta Geodynamica et Geomaterialia*, 175 (3): 1-9.
- [7]. Fakhimi, A., Carvalho, F., Ishida, T. and Labuz, J.F. (2002). Simulation of failure around a circular opening in rock. *International Journal of Rock Mechanics and Mining Sciences*, 39, 507-515.
- [8]. Zhu, W.C., Liu, J.S., Tang, C.A., Zhao, X.D. and Brady, B.H. (2005). Simulation of progressive fracturing processes around underground excavations under biaxial compression. *Tunnelling and Underground Space Technology*, 20 (3): 231-247.
- [9]. Zhu, W.C. and Bruhns, O.T. (2008). Simulating excavation damaged zone around a circular opening under hydromechanical conditions. *International Journal of Rock Mechanics and Mining Sciences*. 5 (45): 815-830.
- [10]. Wang, S.Y., Sloan, S.W., Sheng, D.C. and Tang, C.A. (2012). Numerical analysis of the failure process around a circular opening in rock. *Computers and Geotechnics*, 39, 8-16.
- [11]. Zhao, X.D., Zhang, H.X. and Zhu, W.C. (2014). Fracture evolution around pre-existing cylindrical cavities in brittle rocks under uniaxial compression. *Transactions of Nonferrous Metals Society of China*. 24 (3): 806-815.
- [12]. Liu, J.P., Li, Y.H., Xu, S.D., Xu, S. and Jin, C.Y. (2015). Cracking mechanisms in granite rocks subjected to uniaxial compression by moment tensor analysis of acoustic emission. *Theoretical and Applied Fracture Mechanics*, 75, 151-159.
- [13]. Xu, S.D., Li, Y.H. and Liu, J.P. (2017). Detection of cracking and damage mechanisms in brittle granites by moment tensor analysis of acoustic emission signals. *Acoustical Physics*. 63 (3): 359-367.
- [14]. Shokri, T. (2013). Health Monitoring and Crack Source Location in Reinforced Concrete Based on Acoustic Emission. PhD Thesis, University of Miami.
- [15]. Miller, R.K. and McIntire, P. (1987). *Non-Destructive Testing Handbook: Acoustic Emission Testing*. American Society for Nondestructive Testing.
- [16]. Salinas, V., Vargas, Y., Ruzzante, J. and Gaete, L. (2010). Localization algorithm for acoustic emission. *Physics Procedia*, 3 (1): 863-871.
- [17]. Shull, P.J. (2002). *Nondestructive evaluation: theory, techniques, and applications*. CRC press.
- [18]. Vallen CO. (2010). *AMSY-5 Manual*. www.Vallen.de.
- [19]. Tan, X. (2013). *Hydro-mechanical Coupled Behavior of Brittle Rocks: Laboratory Experiments and Numerical Simulations* (Doctoral dissertation, Institute für Geotechnik).
- [20]. Hu, J. and Xu, N. (2011). Numerical analysis of failure mechanism of tunnel under different confining pressure. *Procedia Engineering*, 26, 107-112.
- [21]. Itasca. (2010). *FLAC-3D (Version 5.0) user manual*.
- [22]. Zhou, Z.L., Zhou, J., Dong, L.J., Cai, X., Rui, Y.C. and Ke, C.T. (2017). Experimental study on the location of an acoustic emission source considering refraction in different media. *Scientific Reports* 7, Article number: 7472 (2017).

## مطالعه ناحیه آسیب پیرامون تونل دایره‌ای با استفاده از روش انتشار آوایی

علی دادی گیوشاد، مرتضی احمدی\* و حمیدرضا نجاتی

گروه مکانیک سنگ، بخش مهندسی معدن، دانشکده فنی و مهندسی، دانشگاه تربیت مدرس، ایران

ارسال ۲۰۱۸/۱۲/۱۸، پذیرش ۲۰۲۰/۰۲/۰۱

\* نویسنده مسئول مکاتبات: moahmadi@modares.ac.ir

### چکیده:

یکی از روش‌هایی که برای بررسی ناحیه آسیب دیده در سازه سنگی مورد استفاده قرار می‌گیرد، روش انتشار آوایی است. این روش مبتنی بر دریافت امواج الاستیک ناشی از تغییر شکل و ترک خوردگی توده سنگ اطراف حفریات زیرزمینی است. در این تحقیق، ناحیه آسیب دیده ناشی از حفر فضاهای دایره‌ای در سنگ به روش آزمایشگاهی و روش عددی مورد مطالعه قرار گرفت. برای این منظور، ۳۳ نمونه مکعبی از سه نوع ماده مختلف شامل ماسه سنگ، ملات سیمان گچ و بتن تهیه شد و یک حفره دایره‌ای در مرکز هر نمونه حفر گردید. قطر حفره‌ها ۲۰ یا ۲۵ میلی‌متر در نظر گرفته شد. نمونه‌ها تحت بارگذاری تک محوره و دومحوره با نرخ تنش متفاوت قرار گرفت. در حالت دومحوره برای قرار دادن سنسورهای آوایی (آکوستیک) سه الگوی قرارگیری مورد بررسی قرار گرفت. بهترین الگو قرار دادن سنسورها مشخص شد و آزمونهای دومحوره بر آن اساس انجام شد. در هنگام انجام آزمون رخدادهای آوایی ساطع شده از نمونه ثبت شد. در ادامه اطلاعات آوایی آزمون‌های آزمایشگاهی با استفاده از نرم‌افزار  $FLAC^{3D}$  و کدهای توسعه یافته مکانیابی شد. در ادامه رابطه بین ناحیه آسیب دیده در نمونه‌های آزمایشگاهی که در آن رخدادهای آوایی در طول بارگذاری رخ داده‌اند با المان‌های عددی که به درجه‌ای از تسلیم کششی و برشی رسیده‌اند مورد مطالعه قرار گرفت. نتایج به دست آمده نشان می‌دهد که میزان پارامترهای آوایی تجمعی در نمونه‌های ملات سیمان گچ بیشتر از سایر نمونه‌ها است. در حقیقت هرچه نمونه دانه ریزتر باشد، مقادیر انرژی و کانت تولید شده بیشتر است. همچنین، نتایج نشان می‌دهد که با افزایش فشار جانبی و سرعت بارگذاری، میزان انرژی تجمعی و کانت کاهش می‌یابد.

**کلمات کلیدی:** ناحیه آسیب اطراف تونل، تونل دایره‌ای، روش انتشار آوایی، نرم‌افزار  $FLAC^{3D}$ .